Doi: 10.1007/s11589-009-0091-5

Three-dimensional numerical simulation on the coseismic deformation of the 2008 M_S8.0 Wenchuan earthquake in China*

Feng Li and Jinshui Huang ♣

Mengcheng National Geophysical Observatory, *School of Earth and Space Sciences*, *University of Science and Technology of China*, *Hefei* 230026, *China*

Abstract Based on the finite element numerical algorithm, the coseismic displacements of the Wenchuan M_S8.0 earthquake are calculated with the rupture slip vectors derived by Ji and Hayes as well as Nishimura and Yaji. Except in a narrow strip around the rupture zone, the coseismic displacements are consistent with those from GPS observation and InSAR interpretation. Numerical results show that rupture slip vectors and elastic properties have profound influences on the surface coseismic deformation. Results from models with different elastic parameters indicate that: ① in homogeneous elastic medium, the surface displacements are weakly dependent on Poisson's ratio and independent of the elastic modulus; ② in horizontally homogeneous medium with a weak zone at its middle, the thickness of the weak zone plays a significant role on calculating the surface displacements; ③ in horizontally and vertically heterogeneous medium, the surface displacements depend on both Poisson's ratio and elastic modulus. Calculations of coseismic deformation should take account of the spatial variation of the elastic properties. The misfit of the numerical results with that from the GPS observations in the narrow strip around the rupture zone suggests that a much more complicated rupture model of the Wenchuan earthquake needs to be established in future study.

Key words: **coseismic deformation; Wenchuan earthquake; finite element method; elastic modulus**
CLC number: P313.5 **Document code**: A

1 Introduction

The M_S8.0 Wenchuan earthquake on 12 May 2008 ruptured more than 300 km of the Longmenshan thrust belt on the eastern margin of the Tibetan plateau. Its epicenter determined by China Seismograph Network Center (CSNC) (2008) is located at (31.0°N, 103.4°E). Field surveys have shown that the surface displacement is as large as 7.6 m (corresponding to a horizontal displacement of 6.1 m and a vertical displacement of 4.6 m) in Yingxiu town that is situated in southern part of the rupture; and in Beichuan city, the maximum surface displacement is 6.6 m (a horizontal displacement of 5.7 m and a vertical displacement of 3.4 m). The earthquake fracture zone is characterized by thrust faulting with dextral strike-slip (Wu and Zhang, 2008). Pre- and post-seismic leveling data also indicate that the coseismic uplift of the hanging wall of the Yingxiu-Beichuan-Nanba thrust fault with respect to Pingwu town is as large as 4.7 m (Wang et al, 2009). Detailed analysis of the field surveying also suggested that the rupture process is very complex in different areas along the surface fracture zone (Deng et al, 2008; Ma et al, 2008). Surface displacements derived from GPS observations tell us the deformation caused by the earthquake in the surrounding areas (Figure 1). The Tibetan block and Sichuan basin reveal significant movement in opposite direction, and in areas away from the rupture zone, the eastward movements of Tibetan plateau are larger than the westward movements of the Sichuan basin (CMONOC Group, 2008). Due to no near-fault GPS site before the Wenchuan earthquake on the hanging wall of the Longmenshan rupture zone, the displacement near the rupture zone is under debate. The results from GPS measurements also show that the westward movements of Sichuan block are much larger than the eastward movements of the Tibetan block in a narrow strip around the rupture zone (Figure 1;

* **Received** 17 December 2009; **accepted in revised form** 11 February 2010; **published** 10 April 2010.
♣ **Corresponding author. e-mail**: jshhuang@ustc.edu.cn

CMONOC Group, 2008). Moreover, it can be seen that, from the InSAR interpretation across the Yingxiu town, there is about 160 cm uplift in the epicenter, and about 100 cm downward movement near Lixian and Wolong county (Ge et al, 2008; Qu et al, 2008).

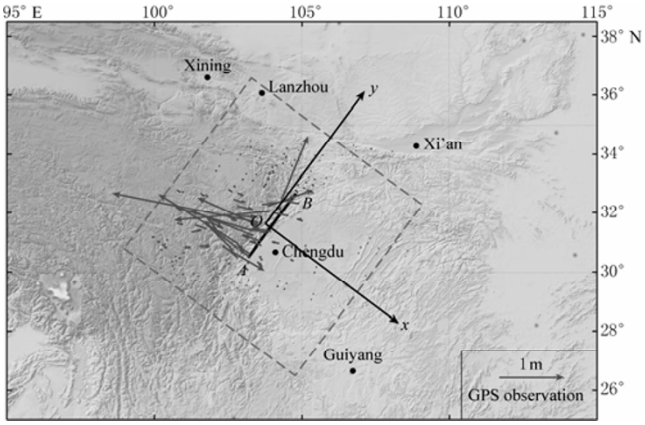

Figure 1 Topographic map showing the rupture zone (segment *AB*) of the Wenchuan M_S8.0 earthquake and the studied area (the square frame specified by dashed lines) of our numerical model. Superimposed are GPS observations (gray lines with arrows) based on CMONOC Group (2008). The horizontal coordinate system *Oxy* is shown with *y* axis parallel to the rupture fault and the origin *O* is about 13.8 km away from the fault.

Models of the rupture process of the Wenchuan earthquake based on body wave and surface wave inversion suggested that the rupture initiated underneath Yingxiu town of Wenchuan county and stopped at Qingchuan county, northeast of the epicenter. The maximum dislocation occurred in vicinity of Wenchuan county and Beichuan county. The process is consisted of two main stages. The first is dominated by thrusting and the second by right-lateral strike-slipping, which is consistent with the complex strike-slip and thrust motion that characterizes the region (Ji and Hayes, 2008; Nishimuru and Yaji, 2008; Wang et al, 2008; Zhang et al, 2009b). Figure 2 shows the rupture process derived by Ji and Hayes (2008) and Nishimuru and Yaji (2008), respectively. Both models indicate that the rupture process is dominated by thrusting near Yingxiu town and right-lateral strike-slipping near Beichuan city (Figure 2). The prominent differences between these two models are: ① the largest movement of the rupture in the model of Ji and Hayes (2008) is much deeper than that in the model of Nishimuru and Yaji (2008); ② the depth of the rupture zone in the former model is much shallower than that in the latter; ③ the second rupture in the latter model is much weaker than that in the former (Figure 2). These two models will be used in our numerical simulation for convenience and simplicity.

The coseismic surface displacements are closely related to the earthquake rupture process. There are a lot of studies on how to determine rupture process from coseismic deformation (Chen et al, 1975; Anzidei et al, 2009; Shen et al, 2009; Wang, 2009; Xu et al, 2009; Zhang et al, 2009a). Because the earthquake rupture process can also be derived from body and surface wave inversion and it is much more precise, many works focused on the calculation of surface deformation from a given rupture process (Huang and Gu, 1982; Okada, 1991; Shen et al, 2008; Zhang and Wei, 2009; Zhang et al, 2009b). For the Wenchuan earthquake, several groups calculated the coseismic deformation with the homogeneous and isotropic elastic half-space models (Shen et al, 2008; Zhang et al, 2009b) or horizontal homogeneous models (Zhang and Wei, 2009). All these help to understand the relationship between the coseismic deformation and the earthquake rupture process.

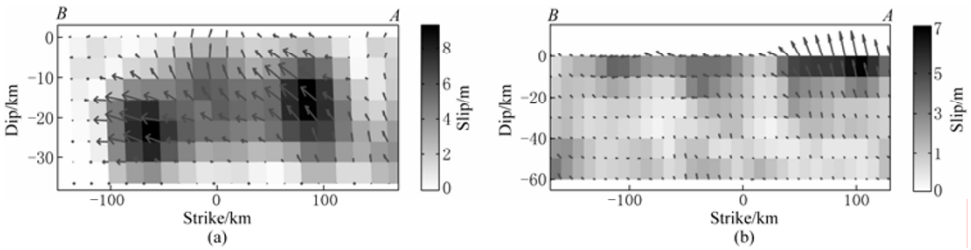

Figure 2 Static slip distribution of the Wenchuan M_S8.0 earthquake from Ji and Hayes (2008) (a) and Nishimuru and Yaji (2008) (b). The strike and dip show distance from our model origin along the strike and dip direction of the rupture fault plane. *A* and *B* correspond to the fault zone shown in Figure 1. The motion of the hanging wall relative to the footwall is indicated by arrows and the slip amplitudes are also shown in gray scale.

However, as the two walls of the Longmenshan thrust fault, Tibetan block and Sichuan basin show large differences in elastic material properties as reported in seismological investigations (e.g., Wang et al, 2003;

Burchfiel et al, 2008; Chang et al, 2008; Zhang et al, 2008b; Lou et al, 2009). Tibetan block belongs to the Tibetan plateau which is a highly active tectonic region, and the Sichuan basin is lying in the Yangtze block which is part of the South China craton. The lithosphere under the Sichuan basin is with higher than average P and S wave velocities because it is a relatively strong cratonic root (Burchfiel et al, 2008). With a joint analysis of teleseismic P-wave receiver functions and Bouguer gravity anomalies, Lou et al (2009) found that there is a lower velocity zone in the lower crust beneath the Songpan-Garze area, while the lower crust underneath Sichuan basin has a relatively high P-wave velocity and density. Surface-wave tomography and receive function analysis on regional arrays in eastern Tibet also suggested that there is a low S-wave velocity zone in the middle and lower crust of Tibetan plateau (Wang et al, 2003; Zhang et al, 2008b). Therefore, we should take account of the heterogeneities in the crust and mantle in the algorithms for calculating surface displacement with a given earthquake rupture process.

This paper aims to set up a three-dimensional numerical model, in which the heterogeneities in the crust and mantle are taken into consideration, to calculate the coseismic deformation caused by the Wenchuan earthquake. The coseismic surface displacements (CMONOC Group, 2008) and the earthquake rupture process (e.g., Ji and Hayes, 2008; Nishimuru and Yaji, 2008) are related directly through material properties such as elastic modulus and Poisson's ratio (e.g., Huang and Gu, 1982; Okada, 1991). Therefore, it is the most important task in this paper to explore the effects of different fault slip vectors and choice of material elastic properties on coseismic deformation. In the following sections, we first explain the setup of our model, and then present the coseismic displacement caused by the Wenchuan earthquake as well as the discussions on the influence of slip vectors. Section 4 mainly focuses on the discussion on the influences of different choices of material properties. Conclusions are given in section 5.

2 Model setup

The static coseismic deformation in a finite volume Ω bounded by surface S is controlled by the following equations (Fu and Huang, 2001):

$$\begin{cases} \dfrac{\partial \sigma_{ij}}{\partial x_j} + f_i = 0 & \text{in } \Omega \\ \sigma_{ij} n_j = T_{i0} \ \text{ or } \ u_i = u_{i0} & \text{on } S \end{cases} \tag{1}$$

where σ_{ij} is stress tensor, f_i is body force vector, u_i is displacement vector, n_j is the normal of S, T_{i0} and u_{i0} are traction and displacement on the surface S, respectively. The stress and displacement are related by

$$\begin{cases} \varepsilon_{ij} = \dfrac{1}{2}\left(\dfrac{\partial u_i}{\partial x_j} + \dfrac{\partial u_j}{\partial x_i} \right) \\ \sigma_{ij} = \lambda \varepsilon_{ij} \delta_{ij} + 2\mu \varepsilon_{ij} \end{cases} \tag{2}$$

where ε_{ij} is strain tensor, λ and μ are Lame parameters, δ_{ij} is the Kronecker delta. The Lame parameters relate to the elastic modulus E and Poisson's ratio ν, and the P- and S-velocity, v_P, v_S, as (Turcotte and Schubert, 2002)

$$E = \frac{(3\lambda + 2\mu)\mu}{\lambda + \mu} \qquad \nu = \frac{\lambda}{2(\lambda + \mu)} \tag{3}$$

and

$$v_P = \sqrt{\frac{\lambda + 2\mu}{\rho}} \qquad v_S = \sqrt{\frac{\mu}{\rho}}, \tag{4}$$

where ρ is density. Equations (1) and (2) are solved with the finite element parallel supported three-dimensional code Pylith, which is available from http://www.geodynamics.org/cig/software/packages/short/pylith. In the code, fault interfaces are used to create jumps in the displacement field (or dislocations) in numerical models. Dislocations arise from slip across the fault surfaces.

Our model is in Cartesian geometry, and its surface is an 800 km×800 km square and its thickness is 100 km. The origin is at the center of the surface area. The y axis is parallel to the strike of the Longmenshan fault with northeast (N49°E) being positive, the x axis is perpendicular to the strike (S41°E) (Figure 1), and the z axis is positive downward (Here it should be noted that the vertical displacement is positive upward). The origin of the coordinate system is about 13.8 km away from the Longmenshan fault. The numerical resolution is 20 km× 20 km. The fault interface is imposed according to the parameters given by Ji and Hayes (2008) or Nishimuru and Yaji (2008). Because we have chosen the strike of the Longmenshan fault as the direction of y axis, the trace of the surface intercepted by the Longmenshan fault in our model is with x=−13.8 km. The dip of the fault interface is set to 33 degrees (Ji and Hayes, 2008; Nishimuru and Yaji, 2008). The rupture zone and slip vectors are prescribed based on that derived by Ji and Hayes (2008) or Nishimuru and Yaji (2008) according to the purpose of this study, which will be mentioned when used. The boundary conditions are traction-free on

the top and no-displacement on the bottom and all side walls.

The studied area is divided into two blocks by the fault interface: the west Tibetan block and east Sichuan block. Seismological inversions suggested that the lower crust of the Tibetan plateau is weak and the west part of China has a thick crust (Wang et al, 2003; Burchfiel et al, 2008; Chang et al, 2008; Zhang et al, 2008b; Lou et al, 2009). Therefore, in our models, the crust is set to be 60 km thick and the upper crust thickness is set to be 18 km. The bottom 40 km is supposed to be mantle lithosphere. The elastic parameters of our model are carefully selected based on the seismological inversions (Wang et al, 2003; Burchfiel et al, 2008; Chang et al, 2008; Zhang et al, 2008b; Lou et al, 2009) and given in Table 1.

Table 1 Parameters for calculating coseismic deformation

Depth h/km	Tibet			Sichuan		
	ρ/kg·m^{-3}	v_S/km·s^{-1}	v_P/km·s^{-1}	ρ/kg·m^{-3}	v_S/km·s^{-1}	v_P/km·s^{-1}
0–18	2 740	3.5	6.0	2 650	3.2	5.5
18–60	2 940	3.0	6.2	2 850	3.7	6.4
60–100	3 250	4.5	7.8	3 150	4.5	7.8

3 Numerical results

3.1 Coseismic deformation of the Wenchuan M_S8.0 earthquake and effect of fault slip vectors

The coseismic deformations of the Wenchuan M_S8.0 earthquake are calculated with the rupture slip vectors derived by Ji and Hayes (2008). The surface horizontal and vertical displacements are shown in Figure 3 and Figure 4, respectively. The horizontal displacements show that there is a significant opposite movement near the rupture zone after the Wenchuan earthquake. The amplitude of the movements decreases with the distance to the rupture zone increasing. The southern part of the rupture zone is characterized by a reverse thrusting and the northern part is dominated by right-lateral strike-slipping (Figure 3), which are generally consistent with the GPS observations (CMONOC Group, 2008). A very striking new phenomenon evident in our model is the rotational movement in the north-west part of our model (Figure 3). This is caused by the varied fault slip vectors and also is consistent with GPS and field observables (Burchfiel et al, 2008; CMONOC Group, 2008; Deng et al, 2008; Ma et al, 2008; Wang et al, 2008; Wu and Zhang, 2008; Zhang et al, 2008a; Zhang et al, 2009b).

As shown in Figure 4a, the vertical displacements are also consistent with that from GPS and InSAR

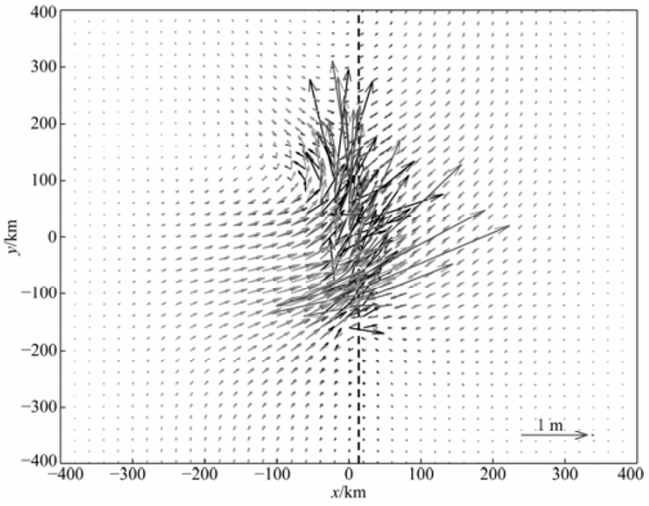

Figure 3 Horizontal coseismic displacements of the numerical model. Dark and light gray arrows represent results based on the rupture slip vectors from Ji and Hayes (2008) and Nishimuru and Yaji (2008), respectively. Vertical dashed line shows the fault interface at the surface which divides the model into two parts, the western Tibet and eastern Sichuan part.

interpretations (CMONOC Group, 2008; Ge et al, 2008; Qu et al, 2008). Near the rupture zone, the displacements in a narrow strip to the west of the fault are mainly upward and their amplitude can be larger than 100 cm. The displacements produce a swell in this narrow strip. The displacements in the two sides of this swell are mainly downward (Figure 4a). The downward movements in the west side of the swell can be larger than 40 cm, while that in the east side is smaller and only about 20 cm. This pattern about the vertical displacements are similar to that inferred from InSAR images, but the amplitudes of the vertical displacements near the rupture zone are smaller when compared with that from InSAR (Figure 4a, Qu et al, 2008).

Although the coseismic deformation is generally consistent with the GPS observations, there is still a significant difference between the horizontal displacement in our model and that from GPS observations (Figure 5a). For example, in the GPS observation, the westward movements of the Sichuan basin is larger than the eastward movements of the Tibetan plateau, which is opposite in our model. This discrepancy is confined to a narrow strip around the rupture zone (Figure 5a). In order to clarify this discrepancy, the fault slip vectors derived by Nishimuru and Yaji (2008) are employed to test the effects of different fault slip vectors on the coseismic deformation. The horizontal and vertical displacements

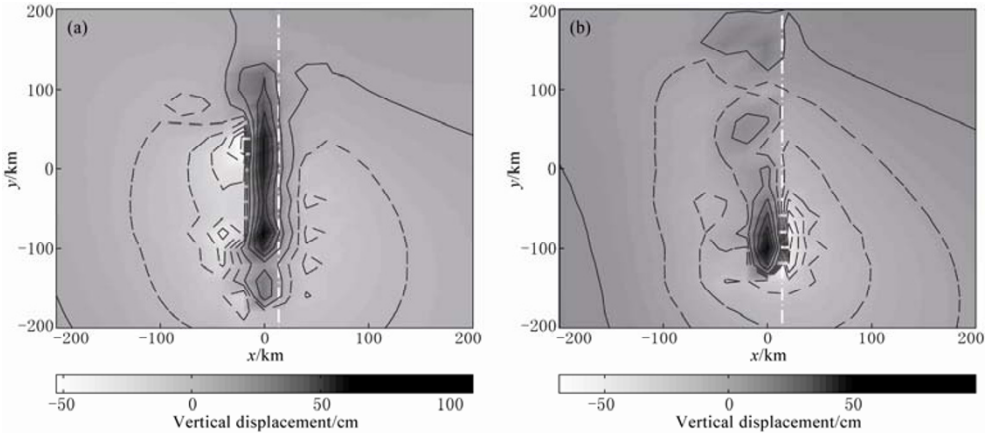

Figure 4 Vertical coseismic displacement of the numerical model in this paper based on the fault slip vectors from Ji and Hayes (a) and Nishimuru and Yaji (b). Superimposed are contour lines. Dashed lines represent negative values and the contour levels are −10, −20, −30, −40, −50 and −60, while solid lines stand for non-negative values with contour levels of 0, 20, 40, 60, 80 and 100. The white dash-dotted lines show the position of the fault interface.

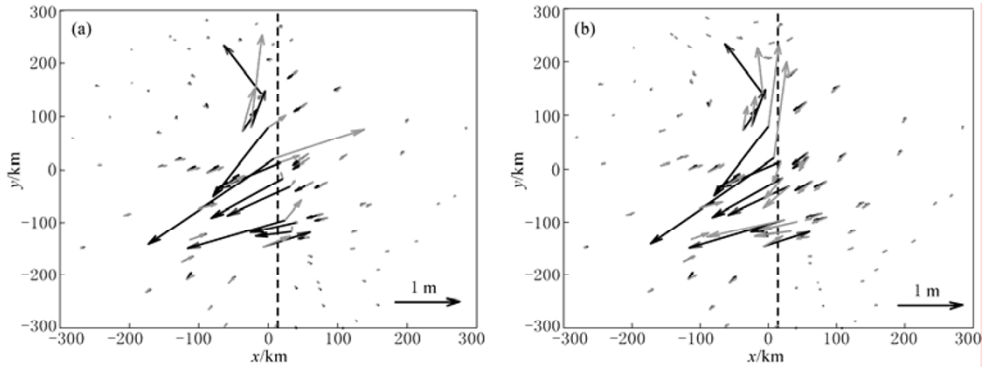

Figure 5 Coseismic horizontal displacements of the numerical models in this paper (denoted by gray arrows) and that from GPS observation (denoted by dark arrows). (a) is based on the fault slip vectors from Ji and Hayes (2008) and (b) is Nishimuru and Yaji (2008). Dashed line shows the position of the fault interface.

are shown in Figure 3 and Figure 4b. Figure 5b shows their differences with the GPS observations.

The differences in the horizontal and vertical displacements between the two models are evident near the rupture zone (Figures 3 and 4b). Because the largest slip of Nishirumu and Yaji's model is on the surface near Yingxiu town, the horizontal surface displacements are larger in this area compared with that from Ji and Hayes's model (Figure 3). The vertical displacements in the northern part of the rupture zone are pretty small (Figure 4b), which are also consistent with the slip model that shows little thrusting in the northern part (Figure 2b). For the results based on Nishirumu and Yaji's model, while the consistency of horizontal displacement with that from the GPS observations getting improved, the discrepancy near the rupture zone is still significant (Figure 5b), and the consistency of the vertical displacements with that from InSAR becomes worse even in southern part of the rupture zone (Qu et al, 2008). It can be seen from Figure 4b that in the southern part, the downward movements in Sichuan basin are larger than that in Tibetan block, which is inconsistent with the InSAR results. The results from InSAR show that the downward movements in Sichuan basin are smaller than that in Tibetan block (Qu et al, 2008).

3.2 Effects of material elastic properties on coseismic deformation of the Wenchuan earthquake

In order to find the reason which causes the discrepancies between the results of the numerical models and that from GPS and InSAR, here we perform a systematic study about the effects of elastic properties. Three groups of tests are included in the following. In each group of the tests, the effects of elastic parameters on the coseismic deformation are tested by varying the

Lame parameters (λ, μ), or the elastic modulus (E) and Poisson's ratio (ν). In this paper, λ ranges between 7.4×10^9 Pa and 4.0×10^{10} Pa, and μ is between 2.0×10^{10} Pa and 4.0×10^{10} Pa; E is between 5.0×10^{10} Pa and 10.0×10^{10} Pa, and ν is between 0.125 and 0.333. In all tests, slip vectors of the rupture process are the same as that in Ji and Hayes (2008).

3.2.1 Effect of material elastic properties in homogeneous medium

The first group of tests is mainly performed to clarify the effects of material elastic properties on the coseismic deformation in a homogeneous medium. Some results of the tests are shown in Figure 6 and the parameters used for this group of tests are listed in Table 2. From now on, only two profiles of the results are selected to discuss: one is at y=80 km (i.e., across the northern part of the rupture zone) and the other is at y=−100 km (i.e., across the southern part of the rupture zone). The northern part is characterized by strike-slip and the southern part is dominated by thrusting. These two profiles are good representatives of our models. Figure 6 shows the three components (U, V, W) of the displacements in x, y, z directions along the two profiles.

Figure 6 shows that, in the northern profile, the displacements perpendicular to the fault (U) of the Sichuan basin and that of the Tibetan plateau are small and comparable (Figure 6a); the displacements along the fault (V) in Tibetan plateau are much larger than that in Sichuan basin (Figure 6b); the upward and downward vertical displacements (W) in Tibetan block are larger than that in Sichuan block (Figure 6c). These are characteristics of deformations of a strike-slip fault with some reverse movement (Huang and Gu, 1982).

Table 2 Elastic parameters in homogeneous medium

No.	λ/GPa	μ/GPa	E/GPa	ν
Case 01	40	40	100	0.250
Case 02	20	40	93	0.167
Case 03	40	20	53	0.333

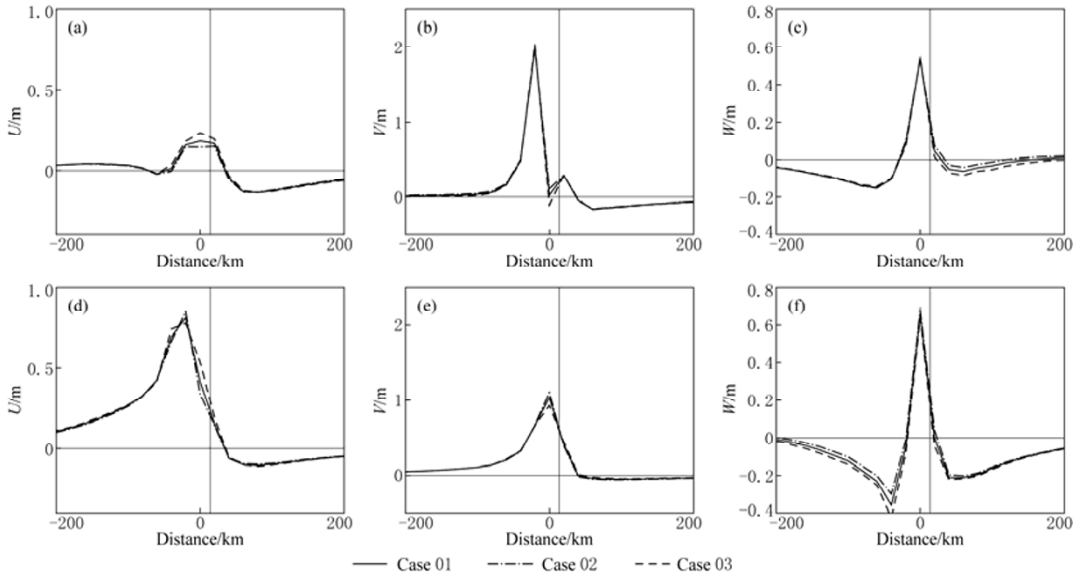

Figure 6 Surface displacements along the profiles y=80 km (a, b and c) and y=−100 km (d, e and f), which are perpendicular to the Longmenshan fault. U and V represent the horizontal displacement perpendicular to the fault and along the fault strike, respectively, while W is the vertical displacement. The vertical and horizontal lines show the place of the Longmenshan fault and the zero values, respectively.

In the southern profile, the displacements U and W are larger but the displacements V are smaller than that in the northern part (Figure 6). Also, the displacements V and the upward and downward vertical displacements W in Tibetan plateau are larger than that in Sichuan basin (Figures 6e and 6f), which are similar to that in the northern part (Figures 6b, 6c, 6e and 6f). However, the displacements U in Tibetan plateau is larger than that in Sichuan basin (Figure 6d), which is different from that in the northern part (Figures 6a and 6d). These are characteristics of deformations of a thrust fault with some strike-slip movement (Huang and Gu, 1982).

In a homogeneous medium, the influences of the elastic material properties are very limited. The influences in cases with a half value of each of the Lame pa-

rameters (λ, μ) are less than 15% (case 01 to case 03, Figure 6). It is worth noting that the λ and μ have different influence on the surface coseismic deformation. Both reducing shear modulus, μ, and Lame parameter, λ, cause little change in the vertical movements of the hanging wall in the northern profile and the footwall in the southern profile (Figures 6c and 6f). However, for the footwall of the northern profile and hanging wall of the southern profile, reducing μ leads to increases in the downward movements; on the contrary, decreasing λ results in decreases in the vertical movements (Figures 6c and 6f).

By converting the Lame parameters, λ, μ, to Young's modulus, E, and Poisson's ratio, ν, we find that, in homogeneous media, the coseismic deformation is independent of the elastic modulus but slightly depend on the Poisson's ratio. The analytic solution of coseismic deformations supports these results (Huang and Gu, 1982).

3.2.2 Effect of material elastic properties in horizontally homogeneous medium

The coseismic deformation shows less dependence on the material elastic properties in a homogeneous medium. In this section, we set up another group of tests to test the influences of material elastic properties on the coseismic deformation in media with vertical changes in elastic properties. Chang et al (2008) and Zhang et al (2008b) pointed out that there is a weak lower crust under Tibetan plateau. Therefore, in this section, we mainly discuss influences of the weak lower crust on the coseismic deformation. For this purpose, our models are divided into three layers: upper crust, lower crust and mantle lithosphere. Because in the western China, e.g., Tibetan plateau, there is always a thick crust, we set the thickness of crust to be 60 km. The thickness of the upper crust is supposed to be 18 km. Therefore, the thickness of the mantle lithosphere is 40 km in most of our models. To test the effects of the thickness of weak lower crust, two models with a crust thickness of 30 km and 70 km are included in this group of tests. The parameters used in some cases of this group of tests are given in Table 3, and the results are shown in Figure 7.

Table 3 Elastic parameters of horizontally homogeneous medium

No.	Depth/km	λ/GPa	μ/GPa	E/GPa	ν
Case 07	0–18	40	40	100	0.250
	18–60	40	40	100	0.250
	60–100	60	60	150	0.250
Case 09	0–18	40	40	100	0.250
	18–60	40	20	53	0.333
	60–100	60	60	150	0.250
Case 13	0–18	40	40	100	0.250
	18–30	20	20	50	0.250
	30–100	60	60	150	0.250
Case 14	0–18	40	40	100	0.250
	18–70	20	20	50	0.250
	70–100	60	60	150	0.250

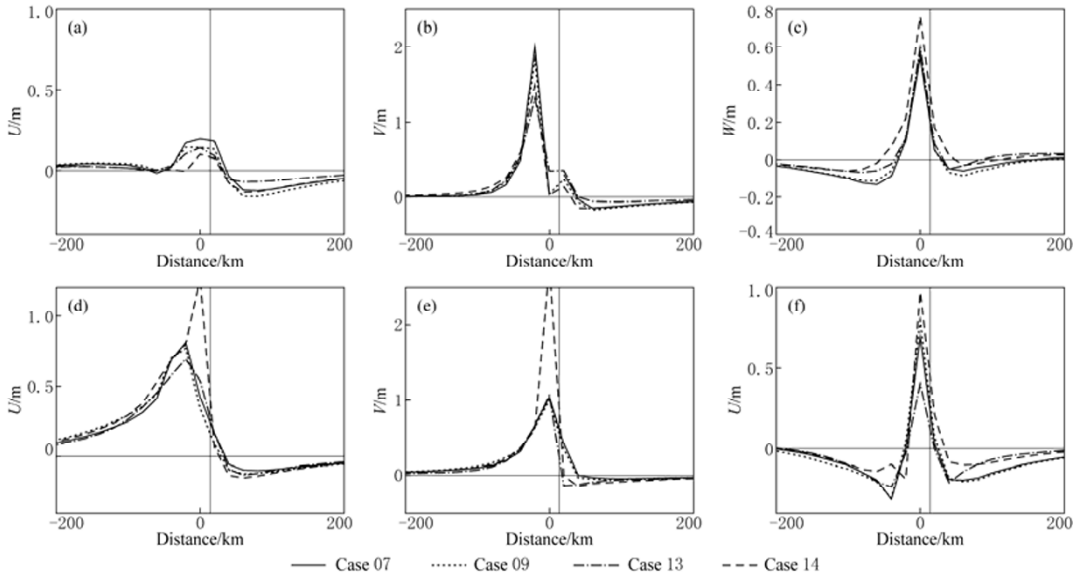

Figure 7 Surface displacements along the profiles y=80 km (a, b and c) and y =−100 km (d, e and f) for case 07, case 09, case 13 and case 14. See captions in Figure 6.

In a horizontally homogeneous medium, the elastic parameters have very small effect on the coseismic de-

formation if the thicknesses of the layers are constant (case 07 and case 09 in Figure 7). The λ and μ have the same influence on the coseismic deformations as that in a homogeneous medium. However, the thickness of the weak lower crust influences the coseismic deformations significantly (Figure 7). This influence is much stronger for thrust fault than for strike-slip one. Figure 7 also shows that, the influences in the southern profile with thrusting fault dominated are much stronger than that in the northern profile, where strike-slipping is dominated. But the patterns of the surface deformation are similar to each other. For example, in the southern profile, the displacements U and V of the Tibetan plateau are larger than that of the Sichuan basin (Figures 7d and 7e); the upward vertical displacements W are mainly in Tibetan block, and in each side of this swell are downward movements (Figure 7f). Therefore, the westward movements of the Sichuan basin are still less than the eastward movements of the Tibetan plateau in this group of tests.

3.2.3 Effect of material elastic properties in horizontally heterogeneous medium

Seismological studies have indicated that there are a lot of differences between Tibetan plateau and the Sichuan basin (Wang et al, 2003; Chang et al, 2008; Zhang et al, 2008b). The Tibetan block might be weak because Tibetan plateau is part of the active tectonic setting and Sichuan basin is part of the Yangtze craton (Burchfiel et al, 2008). The main purpose of this section is to test how a weak Tibetan block influences the coseismic deformation resulted from the Wenchuan earthquake. A case with both horizontal and vertical variations in the elastic parameters is also included in this group of tests. Parameters for some of this group of tests are listed in Table 4, and the corresponding results are shown in Figure 8.

Table 4 Parameters of horizontally heterogeneous medium

No.	Block	Depth/km	λ/GPa	μ/GPa	E/GPa	ν
Case 17	Tibet		20	20	50	0.250
	Sichuan		40	40	100	0.250
Case 19	Tibet		0.74	22	50	0.125
	Sichuan		40	40	100	0.250
Case 20*	Tibet	0–18	40	40	100	0.250
		18–60	20	20	50	0.250
		60–00	60	60	150	0.250
	Sichuan	0–18	40	40	100	0.250
		18–60	40	40	100	0.250
		60–100	60	60	150	0.250

* There are three layers for Tibet and Sichuan in case 20.

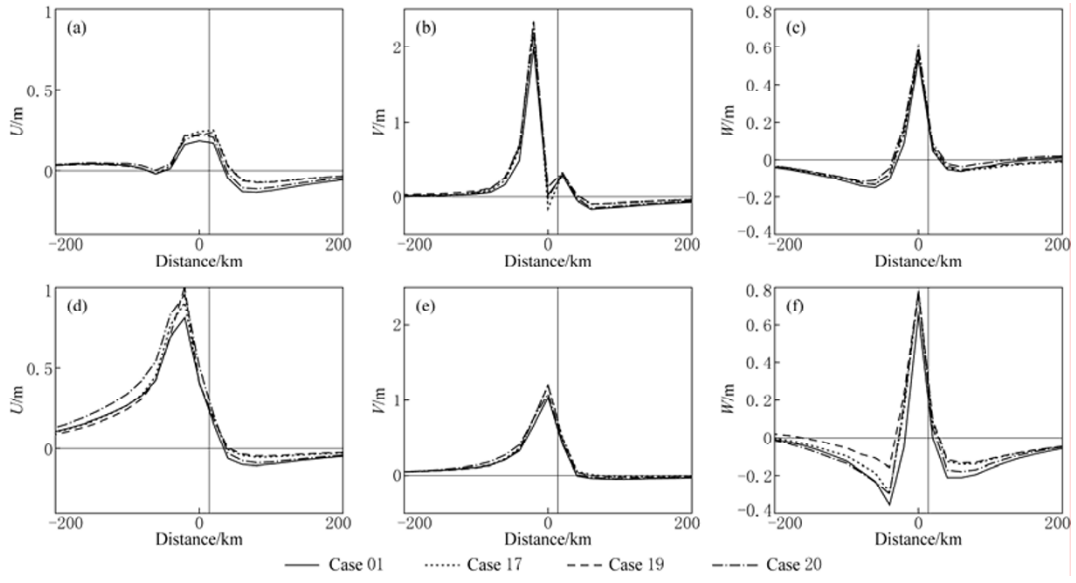

Figure 8 Surface displacements along the profiles y=80 km (a, b and c) and y=—100 km (d, e and f) for case 01, case 17, case 19 and case 20. See captions in Figure 6.

In a horizontally heterogeneous medium, if Tibetan and Sichuan blocks are both homogeneous, the elastic modulus have larger effect on the coseismic deformations than that in a homogeneous or horizontally homogeneous medium. When reducing the elastic modulus and the Poisson's ratio simultaneously, the changes in the vertical displacements in Tibetan plateau are much more evident (Figure 8f). Combination of horizontal and vertical variations in elastic parameters also causes significant changes in the coseismic deformation, which is much apparent for horizontal displacements in the southern part of the rupture zone (Figure 8d).

The above results show that the elastic properties have profound influences on the coseismic deformations of the Wenchuan earthquake. But with the parameter space we tested in this study, the westward movements of the Sichuan basin are always less than the eastward movements of the Tibetan plateau in the narrow strip around the rupture zone (Figure 3), which is inconsistent with that from the GPS observations (CMONOC Group, 2008). This suggests that the complicated rupture process might not be simplified to a single fault rupture as did by Ji and Hayes (2008) or Nishimuru and Yaji (2008). Therefore, it is needed to take account of the ruptures in the parallel sub-faults (Deng et al, 2008; Zhang et al, 2008a) or a rupture process on a listric fault in future studies.

4 Discussion and conclusions

In this paper, we calculated the coseismic deformation of the Wenchuan M_S8.0 earthquake with the three dimensional finite element code Pylith. Although inconsistent with that from GPS observations (Figure 5) in a narrow strip around the rupture zone, our numerical model is consistent with the GPS observations and InSAR interpretations in broad features (CMONOC Group, 2008; Qu et al, 2008). Four groups of tests, with different rupture slip vectors, different elastic parameters in a homogeneous medium, different elastic parameters in a horizontally homogeneous medium and different elastic parameters in a horizontally heterogeneous medium, respectively, could not reconcile the discrepancy in the narrow trip, which means a further more complicated rupture process need to be constructed.

Numerical results show that, for horizontal displacement, there is a significant opposite movement near the rupture zone after the Wenchuan earthquake. The amplitudes of the movements decrease with the distance to the rupture zone increasing. The southern part of the rupture zone is characterized by a reverse thrusting and the northern part of the rupture zone is dominated by right-lateral strike-slipping. There is a rotational movement in the north-west part of our model (Figure 3). Near the rupture zone, to the west of the fault, there are about 100 cm upward movements, and in both sides of this swell, the displacements are mainly downward with about 40 cm in the west and about 20 cm in east (Figure 4a).

Numerical results also show that the fault slip vectors have profound influences on the coseismic deformation. Both horizontal and vertical displacements based on the fault slip vectors derived by Ji and Hayes (2008) and Nishimuru and Yaji (2008) show significant differences (Figure 3 to Figure 5), suggesting that it may be needed to combine the seismic data and surface deformation information such as the displacements from GPS and InSAR so as to obtain proper fault slip vectors in the future.

The material properties also affect the coseismic deformations. In a homogeneous medium, the surface coseismic deformations only weakly depend on the Poisson's ratio and are independent of the elastic modulus. Similarly, in a horizontally homogeneous medium with a weak zone at the middle, the elastic properties also show less influences on the coseismic deformation once the sizes of each layer is constant. The thickness of the weak layer has great influences on the surface coseismic deformation, which depends on the slip vectors and their changes from one location to another. In a horizontally heterogeneous, but vertically homogenous medium, the dependence of coseismic deformations on the elastic parameters is also weak. However, in a horizontally heterogeneous medium with a weak middle layer, the coseismic deformation could significantly depend on elastic parameters.

Acknowledgements This work was supported by the National Natural Science Foundation of China under grant No. 40774045 and partially supported by the program from Chinese Academy of Sciences under grant No. KZCX2-YW-QN507. Li partially thanks the support from the Graduate Innovation Project, University of Science and Technology of China.

References

Anzidei M, Boschi E, Cannelli V, Devoti R, Esposito A, Galvani A, Melini D, Pietrantonio G, Riguzzi F, Sepe V and Serpelloni E (2009). Coseismic deformation of the destructive April 6, 2009 L'Aquila earthquake (central Italy) from GPS data. *Geophy Res Lett* **36**: L17307, doi:10.1029/2009GL039145.

Burchfiel B C, Royden L H, van der Hilst R D and Hager B H (2008). A geological and geophysical context for the Wenchuan earthquake of 12 May 2008, Sichuan, People's Republic of China. *GSA Today* **18**(7): 4–11.

Chang L J, Wang C Y and Ding Z F (2008). Seismic anisotropy of upper mantle in Sichuan and adjacent regions. *Science in China* (*Series D*) **51**(12): 1 683–1 693.

Chen Y T, Lin B H, Lin Z Y and Li Z Y (1975). The focal mechanism of the 1966 Xingtai earthquake as inferred from the ground deformation observation. *Chinese J Geophys* **18**(3): 164–182 (in Chinese).

China Seismograph Network Center (2008). Source parameters for the M_S8.0 earthquake in Wenchuan, Sichuan. 2008-05-12, http://www.csi.ac.cn/sichuan/sichuan080512_cs1.htm (in Chinese).

CMONOC Group (2008). Coseismic displacements of the 2008 Wenchuan M_S8.0 earthquake from GPS observation. *Science in China* (*Series D*) **38**(10): 1 195–1 216 (in Chinese).

Deng Z H, Yang Z E, Sun Z M, Chen G H, Ma W T and Sun Q (2008). Complicated phenomena of the Beichuan-Yingxiu surface zone during Wen-

chuan M_S8.0 earthquake in Sichuan Province, China. *Chinese Sci Bull* **53**(24): 3 891–3 896.

Fu R S and Huang J H (2001). *Geodynamics*. High Education Press, Beijing, 80–88 (in Chinese).

Ge L L, Zhang K, Ng A, Dong Y S, Chang H C and Rizos C (2008). Preliminary results of satellite radar differential interferometry for the coseismic deformation of the 12 May 2008 M_S8.0 Wenchuan earthquake. *Geographic Information Sciences* **14**(1): 12–19.

Huang L R and Gu G H (1982). *Elastic Static Displacement Theory*. Seismological Press, Beijing, 344 (in Chinese).

Ji C and Hayes G (2008). Preliminary result of the 12 May 2008 M_W7.9 eastern Sichuan, China earthquake. 2008-05-15, http://earthquake.usgs.gov/earthquakes/eqinthenews/2008/us2008ryan/finite_fault.php.

Lou H, Wang C Y, Lu Z Y, Yao Z X, Dai S G and You H C (2009). Deep tectonic setting of the 2008 Wenchuan M_S8.0 earthquake in southwest China — Joint analysis of teleseismic P-wave receiver functions and Bouguer gravity anomalies. *Science in China* (*Series D*) **52**(2): 166–179.

Ma Y S, Long C X, Tan C X, Wang T, Zhang Y S, Lei W Z, Li B, Gong M Q, Liao C T and Wu M L (2008). Co-seismic deformation features and segmentation of the M_S8.0 Wenchuan earthquake in Sichuan, China. *Geol Bull China* **27**(12): 2 076–2 085 (in Chinese with English abstract).

Nishimuru N and Yaji Y (2008). Rupture process for May 12, 2008 Sichuan earthquake (preliminary result). 2008-05-15, http://www.geol.tsukuba.ac.jp/~nisimura/20080512/.

Okada Y (1991). Internal deformation due to shear an tensile faults in a half-space. *Bull Seism Soc Amer* **82**: 1 018–1 040.

Qu C Y, Song X G, Zhang G F, Guo L M, Liu Y H, Zhang G H, Li W D and Shan X J (2008). Analysis on the characteristics of InSAR coseismic deformation of the M_S8.0 Wenchuan earthquake. *Seismology and Geology* **30**(4): 1 076–1 084 (in Chinese with English abstract).

Shen C Y, Li H and Tan H B (2008). Simulation of co-seismic gravity changes and deformation effect of Wenchuan M_S8.0 earthquake. *Journal of Geodesy and Geodynamics* **28**(5): 6–12 (in Chinese with English abstract).

Shen Z K, Sun J B, Zhang P Z, Wan Y G, Wang M, Burgmann R, Zeng Y H, Gan W J, Liao H and Wang Q L (2009). Slip maxima at fault junctions and rupturing of barriers during the 2008 Wenchuan earthquake. *Nature Geoscience* **2**: 718–724.

Turcotte D L and Schubert G (2002). *Geodynamics*. Second edition. Cambridge University Press, Cambridge, 106–108.

Wang C, Wu J, Lou H, Zhou M D and Bai Z M (2003). P-wave crustal velocity structure of crust and mantle from seismic surface wave dispersion in Sichuan-Yunnan region, China. *Chinese J Geophys* **51**(4): 1 114–1 122 (in Chinese with English abstract).

Wang M (2009). Coseismic slip distribution of the 2008 Wenchuan great earthquake constrained using GPS coseismic displacement field. *Chinese J Geophys* **52**(10): 2 519–2 526 (in Chinese with English abstract).

Wang Q L, Cui D X, Zhang X, Wang W P, Liu J W, Tian K and Song Z S (2009). Coseismic vertical deformation of the M_S8.0 Wenchuan earthquake from repeated levelings and its constraint on listric fault geometry. *Earthquake Science* **22**: 595–602.

Wang W M, Zhao L F, Li J and Yao Z X (2008). Rupture process of the M_S8.0 Wenchuan earthquake of Sichuan, China. *Chinese J Geophys* **51**(5): 1 403–1 410 (in Chinese with English abstract).

Wu Z H and Zhang Z C (2008). Seismic deformation and co-seismic displacement of the M_S8.0 Wenchuan earthquake in Sichuan, China. *Geol Bull China* **27**(12): 2 067–2 075 (in Chinese with English abstract).

Xu C J, Liu Y and Wen Y M (2009). M_W7.9 Wenchuan earthquake slip distribution inversion from GPS measurements. *Acta Geodaetica et Cartographica Sinica* **38**(3): 195–215 (in Chinese with English abstract).

Zhang G H, Wang C S, Qu C Y and Shan X J (2009a). Inversion of the coseismic deformation of the M_W8.0 earthquake derived from InSAR technology using sensitivity-based iterative fitting method. *Earthquake* **29**(Suppl.): 113–121 (in Chinese with English abstract).

Zhang K L and Wei D P (2009). The influences of gravitation and viscoelasticity on coseismic and postseismic deformation in the Wenchuan earthquake. *Physics* **38**(4): 254–260 (in Chinese with English abstract).

Zhang P Z, Xu X W, Wen X Z and Ran Y K (2008a). Slip rates and recurrence intervals of the Longmen Shan active fault zone and tectonic implications for the mechanism of the May 12 Wenchuan earthquake. *Chinese J Geophys* **51**(4): 1 066–1 073 (in Chinese with English abstract).

Zhang Y, Feng W P, Xu L S, Zhou C H and Chen Y T (2009b). Spatio-temporal rupture process of the 2008 great Wenchuan earthquake. *Science in China* (*Series D*) **52**(2): 145–154.

Zhang Z, Chen Y and Li F (2008b). Reconstruction of the S-wave velocity structure of crust and mantle from seismic surface wave dispersion in Sichuan-Yunnan region. *Chinese J Geophys* **51**(4): 1 114–1 122 (in Chinese with English abstract).